

## The effect of Laser-Induced deconsolidation on the compaction behavior of thermoplastic composite tapes

Çelik, Ozan; Bussink, Tom; Peeters, Daniël; Teuwen, Julie; Dransfeld, Clemens

**DOI**

[10.1016/j.compositesa.2021.106670](https://doi.org/10.1016/j.compositesa.2021.106670)

**Publication date**

2021

**Document Version**

Final published version

**Published in**

Composites Part A: Applied Science and Manufacturing

**Citation (APA)**

Çelik, O., Bussink, T., Peeters, D., Teuwen, J., & Dransfeld, C. (2021). The effect of Laser-Induced deconsolidation on the compaction behavior of thermoplastic composite tapes. *Composites Part A: Applied Science and Manufacturing*, 151, Article 106670. <https://doi.org/10.1016/j.compositesa.2021.106670>

**Important note**

To cite this publication, please use the final published version (if applicable). Please check the document version above.

**Copyright**

Other than for strictly personal use, it is not permitted to download, forward or distribute the text or part of it, without the consent of the author(s) and/or copyright holder(s), unless the work is under an open content license such as Creative Commons.

**Takedown policy**

Please contact us and provide details if you believe this document breaches copyrights. We will remove access to the work immediately and investigate your claim.



# The effect of Laser-Induced deconsolidation on the compaction behavior of thermoplastic composite tapes

Ozan Çelik<sup>\*</sup>, Tom Bussink, Daniël Peeters, Julie Teuwen, Clemens Dransfeld

Aerospace Manufacturing Technologies, Faculty of Aerospace Engineering, Delft University of Technology, Kluyverweg 1, Delft, 2629HS, the Netherlands

## ARTICLE INFO

### Keywords:

- A. Polymer-matrix composites (PMCs)
- B. Microstructures
- D. Process monitoring
- E. Automated fiber placement (AFP)

## ABSTRACT

The effects of laser-induced deconsolidation on the compaction process of CF/PEEK tapes were investigated. First, tapes with different degrees of deconsolidation were manufactured using a laser heater. This procedure resulted in samples with different waviness, thickness, void content and surface roughness values. Then, as-received and laser-deconsolidated tapes were compacted under two different temperature histories and four different pressure levels. Waviness induced by laser-deconsolidation vanished when the material was heated up to the glass transition temperature even at a very low compaction pressure. Unlike waviness; increased thickness, void content and surface roughness due to laser-deconsolidation remained between the glass transition and melting temperatures. After the melting temperature was exceeded, the effects of laser-deconsolidation were dependent on the applied pressure and initial degree of deconsolidation. The final surface roughness, thickness and degree of effective intimate contact were affected by the degree of laser-deconsolidation when a compaction pressure of less than 300 kPa was applied.

## 1. Introduction

Laser-assisted fiber placement (LAFP) with in-situ consolidation (without a post-consolidation step such as an autoclave, oven or press) has received an increasing attention from composite manufacturing community in the recent years [1]. The method offers precise and repeatable production of near net-shaped thermoplastic composite parts with minimum human intervention [2]. Moreover, skipping the post-consolidation step has the potential for a great reduction in processing time and energy consumption. A typical LAFP system is demonstrated in Fig. 1. Layers of thermoplastic composite material are joined by first heating via a laser heater pointed at the nip point between the incoming tape and underlying substrate and then, compacting with a silicone or metal roller.

The resulting part quality is highly dependent on the short (< 1 s) compaction phase of the process. Several phenomena such as intimate contact development [3–5], void compression [6] and tape deformation [7] take place during the time spent under the compaction roller. These phenomena play a significant role in determining the final mechanical properties, dimensions and porosity of the structure [8,9]; therefore, it is crucial to have a deep understanding on the compaction behavior of the tape during LAFP [10].

As demonstrated in Fig. 1, laser heating changes the micro- and meso-structure of the tape significantly. These changes have been termed as deconsolidation in the literature [11]. Specifically, the laser-deconsolidated tape has a higher waviness, roughness, thickness and volumetric void content than the as-received tape as shown in [12]. The effects of deconsolidation on the compaction of the tape is important due to the limited compaction time during LAFP.

The effects of deconsolidation on the compaction behavior of the thermoplastic composite tapes have been investigated by only few researchers. Kok et al. focused on the influence of fiber decompaction at the tape surface due to laser heating [13]. They showed that laser irradiation may lead to a resin-poor layer at the tape surface and formulated an intimate contact model based on through-thickness impregnation of the dry fibers [14]. The model predicted the experimental results with limited success. The assumption of a one-dimensional problem domain may have led to oversimplification of the intimate contact development phenomenon. Later on, in a previous work of the authors, it was shown that due to the presence of dry fibers at the tape surface, a complete mechanical contact against the opposite surface may not eliminate interlaminar voids or ensure full bond strength development [5]. The concept of effective intimate contact, which is the ratio of the resin material in contact with the opposing

<sup>\*</sup> Corresponding author.

E-mail address: [ozancelik138@gmail.com](mailto:ozancelik138@gmail.com) (O. Çelik).

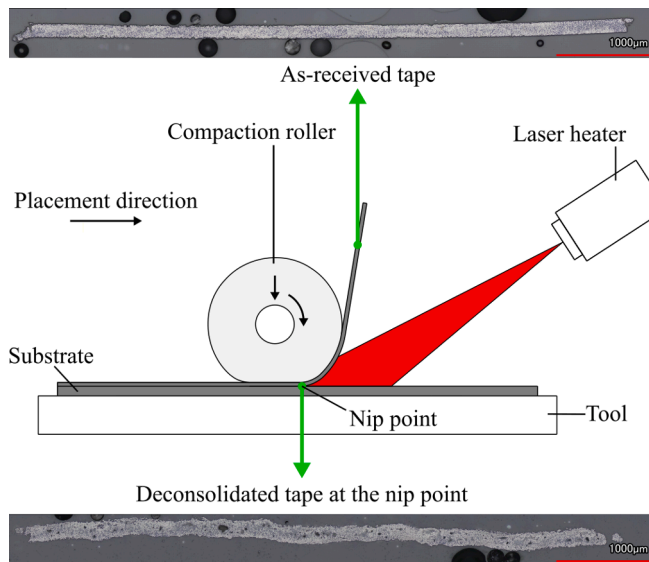


Fig. 1. Working principle of a typical LAFP system with representative cross-sectional images demonstrating how laser heating can alter the microstructure of the composite tape prior to the nip point.

surface to the whole projected surface area, was proposed. Experimental results suggested that effective intimate contact develops as a result of a combination of squeeze flow and percolation flow in both the thickness and fiber directions. In [12], the possible effects of other forms of deconsolidation such as waviness formation, void content increase and non-uniform thickness increase on the compaction of the tape were discussed. It was suggested that these effects should be considered for calculation of heat transfer, void compaction and effective intimate contact development. An experimental study which systematically addresses the effect of deconsolidation under different compaction parameters is not present in the literature. Also, behavior of different degrees of deconsolidation during the compaction process, which is important for LAFP models, has not been investigated yet.

The objective of this study is therefore to understand the differences between the compaction behavior of as-received and laser-deconsolidated tapes exposed to the same temperature and pressure history. To reach this goal, a two-step experimental procedure was performed. First, carbon fiber reinforced polyetheretherketone (CF/PEEK) tapes were deconsolidated using a Vertical-Cavity Surface-Emitting Laser (VCSEL) heater under conditions similar to the heating phase of LAFP. Then, samples from these tapes were compacted under two temperature histories with relatively fast heating/cooling rates, and four pressure levels. As-received tape samples were also compacted as reference. The effects of deconsolidation were studied with in-situ and ex-situ methods. The gap thickness and temperature were measured during the compaction experiments. Cross-sectional microscopy, effective intimate contact measurement and confocal microscopy were employed after the experiments.

## 2. Materials and experimental methods

### 2.1. Materials

The material used in this study was Toray TC1200 CF/PEEK slit in 6.35 mm-wide tapes. The nominal thickness of the as-received tape was 0.15 mm. The glass transition ( $T_g$ ) and melting ( $T_m$ ) temperatures of PEEK were reported as 143 °C and 343 °C, respectively [15].

### 2.2. Deconsolidation of As-received tapes

An experimental setup was designed to deconsolidate CF/PEEK tapes

under conditions similar to the heating phase of LAFP. Fig. 2 demonstrates the setup and its components. A composite tape was attached to an aluminum tool using polyimide tapes at the ends and heated with a laser heater while the temperature at the tape surface was measured with a thermal camera.

A TRUMPF PPM411-12-980-24 laser module with a total output capacity of 2.4 kW was used to heat the surface of the composite tape. The device contains 12 heating zones which can be independently activated and adjusted to get a tailored heating profile. The heater was positioned so that the emitted laser beams were perpendicular to the plane the composite tape lies on. The distance between the laser heater and the tape was 5 cm.

Temperature on the tape surface during heating was measured with a FLIR A655sc long-wave infrared (LWIR) camera. The resolution of the detector of the camera was  $640 \times 480$  pixels. The accuracy of the temperature measurement was  $\pm 2$  °C or  $\pm 2\%$  (whichever is greater). The camera was calibrated in the range of 100–650 °C.

The specimens were deconsolidated at two different laser settings to obtain different degrees of deconsolidation and split into two groups based on the laser settings: highly and slightly laser-deconsolidated samples (HLD and SLD, respectively). The laser settings used for each group of samples are shown in Table 1. The settings were determined so that the HLD samples reached an average temperature over the heated area significantly above the  $T_m$ , whereas the SLD samples reached an average temperature between  $T_g$  and  $T_m$  to limit the effects of deconsolidation. The high scatter in temperature at the tape surface is a result of the varying angle of incidence between the laser beams and the surface features caused by waviness formation during laser heating [12].

### 2.3. Compaction of As-received and deconsolidated tapes

The as-received (ASR), SLD and HLD samples were compacted in a TA Instruments RSA-G2 Solids Analyzer. A compression fixture was installed on the instrument as demonstrated in Fig. 3. 6–7 mm long samples were extracted from the as-received and laser-deconsolidated tapes and placed between two 25 µm-thick Polyimide (Kapton) films to prevent damage to the compression platens. Following that, a heating/cooling cycle was applied on the samples under constant compressive force. The samples were compacted under constant compressive force for two reasons. Firstly, further deconsolidation during the heating or cooling phases of the compaction experiments was prevented by applying a compaction force. Secondly, application of compaction force during the whole temperature history allows one to observe the compaction behavior at different temperature ranges. This is especially important for the LAFP process, where the temperature of the incoming tape might drop below the melting temperature under the compaction roller [16].

Two different compaction settings were used as shown in Table 2. The first group of samples was heated from 25 °C to the target temperature of 400 °C (above  $T_m$ ) with a rate of 60 °C/min, held at that temperature for 20 s and cooled down to 25 °C with a rate of 60 °C/min. The experiments were repeated at four different pressure levels: 10, 50, 100 and 300 kPa. The compaction force was calculated for each experiment by multiplying the desired pressure and the initial projected area of each sample, and kept constant throughout the whole experiment. The second group of samples was heated from 25 °C to the target temperature of 245 °C (between  $T_g$  and  $T_m$ ). The heating/cooling rates and holding duration were the same with the previous set of experiments and the highest ones that could be achieved with the experimental setup. These experiments were performed only at 300 kPa pressure.

The pressure values of the experiments above  $T_m$  were determined to cover a range between the minimum and maximum compaction forces which could be reliably achieved with the instrument. During the LAFP process, the pressure under the compaction roller is dependent on the roller geometry and material as well as the applied compaction force. A pressure of 300 kPa was reached by applying a compaction force of 100

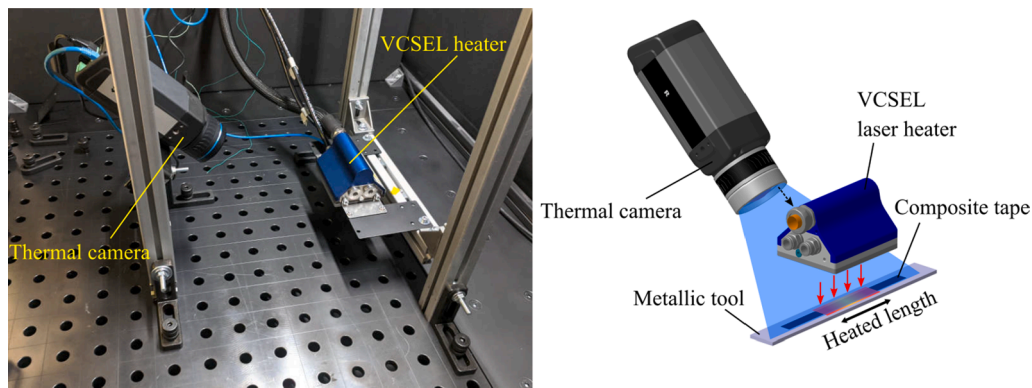


Fig. 2. Experimental setup for laser-deconsolidation of composite tapes.

Table 1

Laser settings used in deconsolidation experiments.

Specimen group	Activated zones	Total power (W)	Time (ms)	Max. average temperature ( °C)	Max. local temperature ( °C)
Highly laser-deconsolidated (HLD)	1–11	550	800	395–511	448–566
Slightly laser-deconsolidated (SLD)	1–11	286	800	232–296	268–341

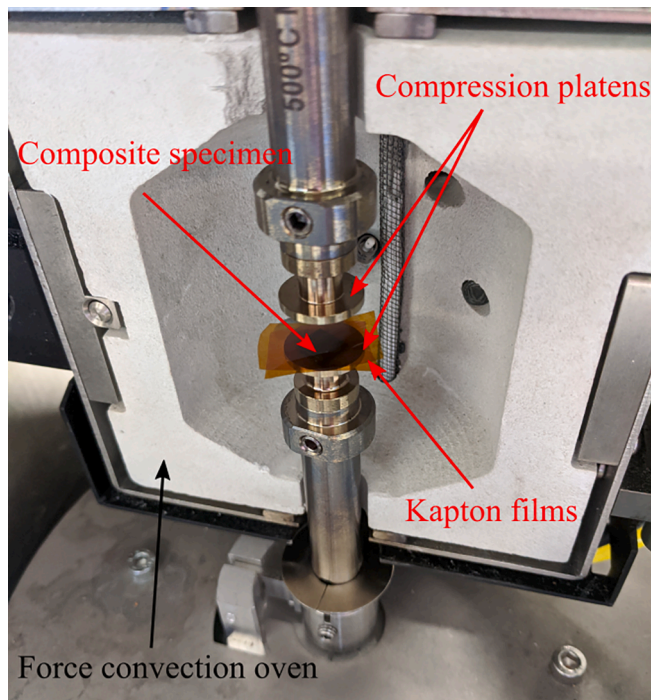


Fig. 3. Experimental setup for compaction of composite tapes.

N on a flat surface using a roller with a hardness of Shore A 60 and a diameter of 70 mm [5]; however, the same pressure was obtained for a compaction roller with a hardness of 20HA and a diameter of 80 mm when a compaction force of 800 N was applied [17]. Also, pressures lower than 300 kPa can be observed on convex surfaces [17].

The target temperature set in the instrument represents the

Table 2

Parameters used in the compaction experiments.

Specimen group	Heating rate ( °C/min)	Target temperature ( °C)	Soak time (s)	Cooling rate ( °C/min)	Max. thermocouple ( °C)	Pressure (kPa)
Above $T_m$	60	400	20	60	363	10, 50, 100 and 300
Above $T_g$	60	245	20	60	200	300

temperature of the gas circulating in the convection oven. Due to the relatively fast heating/cooling cycle and the lack of time to equilibrate with the environment, the temperature of the objects between the compression platens differs from the gas temperature. To determine the actual sample temperature during the experiments, a 100  $\mu\text{m}$ -thick K-type thermocouple was placed between two Kapton films and compacted with the settings explained above. As shown in Fig. 4, the temperature measured with the thermocouple lagged behind the programmed target temperature and reached 363 °C and 200 °C at its peak for the target temperatures of 400 and 245 °C, respectively. In this work, the temperature history measured with the thermocouple was used as the reference temperature throughout the compaction process.

Due to the presence of the Kapton tapes between the platens, the gap thickness measured during the experiments needed to be corrected to obtain the net gap thickness associated with the composite specimen. To do that, a reference experiment was performed with only two Kapton films between the compression platens before each experiment. The reference gap thickness was recorded during the compaction cycle. Three repetitions were performed for each degree of deconsolidation and temperature/pressure combination in Table 2 and the average reference gap thickness was calculated for each combination. Following that, the actual experiment including the composite tape was completed (also performed for three specimens). The average reference gap thickness was subtracted from the gap thickness of each actual experiment to obtain the net gap thickness. Finally, the three net gap thickness curves were aligned in the time axis and averaged to obtain a single net gap thickness curve for each combination of the degree of deconsolidation, temperature and pressure. These gap thickness curves are demonstrated in Fig. 5.

#### 2.4. Degree of effective intimate contact

Degree of effective intimate contact (DEIC), which was defined as the amount of compacted resin at the tape surface, was measured using the methodology provided in [5]. A Keyence VHX-2000 optical microscope

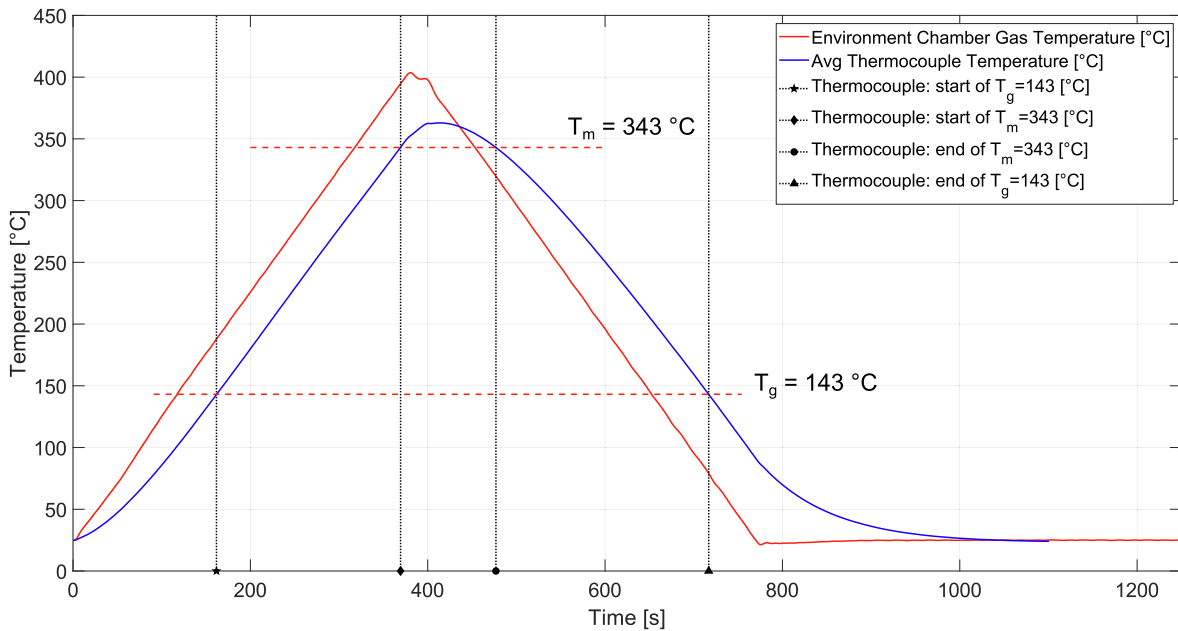


Fig. 4. The gas temperature programmed in the software of the compaction set-up and the temperature measured with a thermocouple placed between two Kapton films.

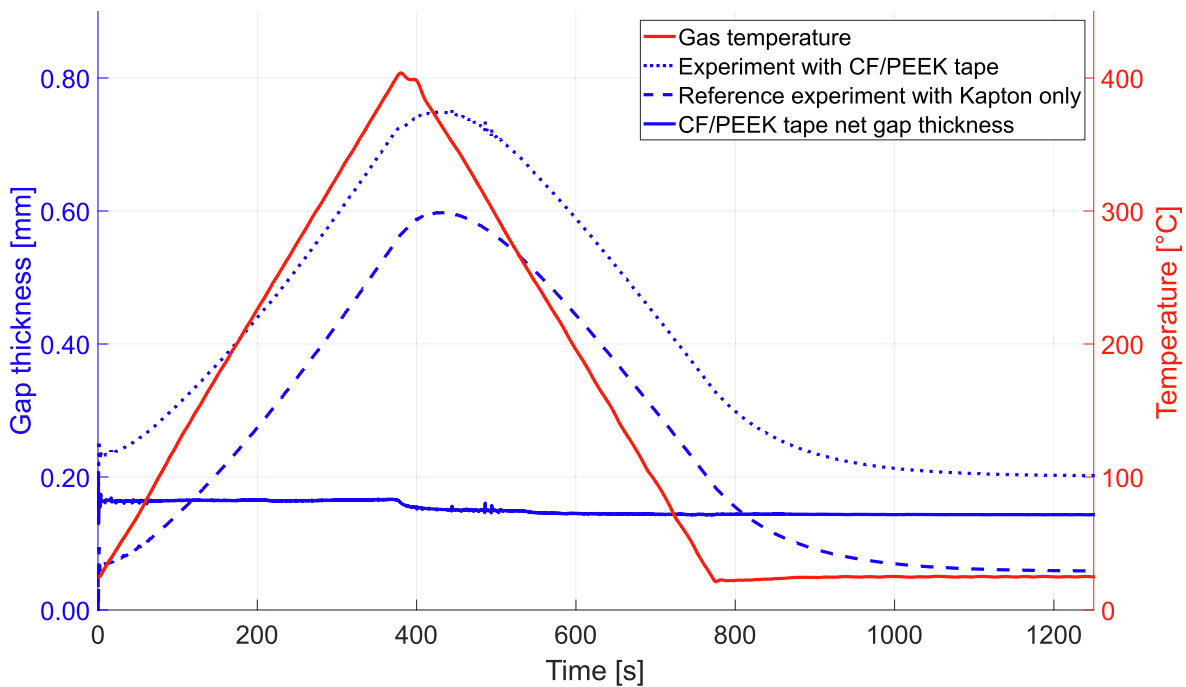


Fig. 5. Representative gas temperature along with the corresponding gap thicknesses from the experiment with CF/PEEK tape, the reference experiment with Kapton tape only, and the calculated net gap thickness of the CF/PEEK sample.

equipped with a VH-Z100 lens was used to capture the whole surface of the specimens after the compaction tests (demonstrated in Fig. 6a). These images were converted to grayscale images and a grayscale histogram was generated for each image (Fig. 6c). In these histograms, two clear peaks were present representing the dry fibers (the peak with the lower grayscale value) and the compacted resin area (the peak with the higher grayscale value). A threshold was chosen at the local minimum between the two peaks. The pixels with a grayscale value higher than this threshold were selected. Visual inspection showed that the selected area included a low amount of dry fibers. To eliminate them from the selected area, all sub-areas smaller than  $500 \mu\text{m}^2$  were excluded

(Fig. 6b). DEIC was calculated as the ratio of the remaining resin-rich area at the surface to the whole area of the image.

### 2.5. Cross-sectional microscopy

The final void content and thickness of the composite specimens after the compaction tests were determined by cross-sectional microscopy. Also, additional samples were cut from the composite tapes to represent the state of the specimens prior to the compaction tests. The specimens were embedded into slow-curing mounting epoxy (Struers Epofix) and ground/polished in a Struers Tegramin-20 specimen preparation

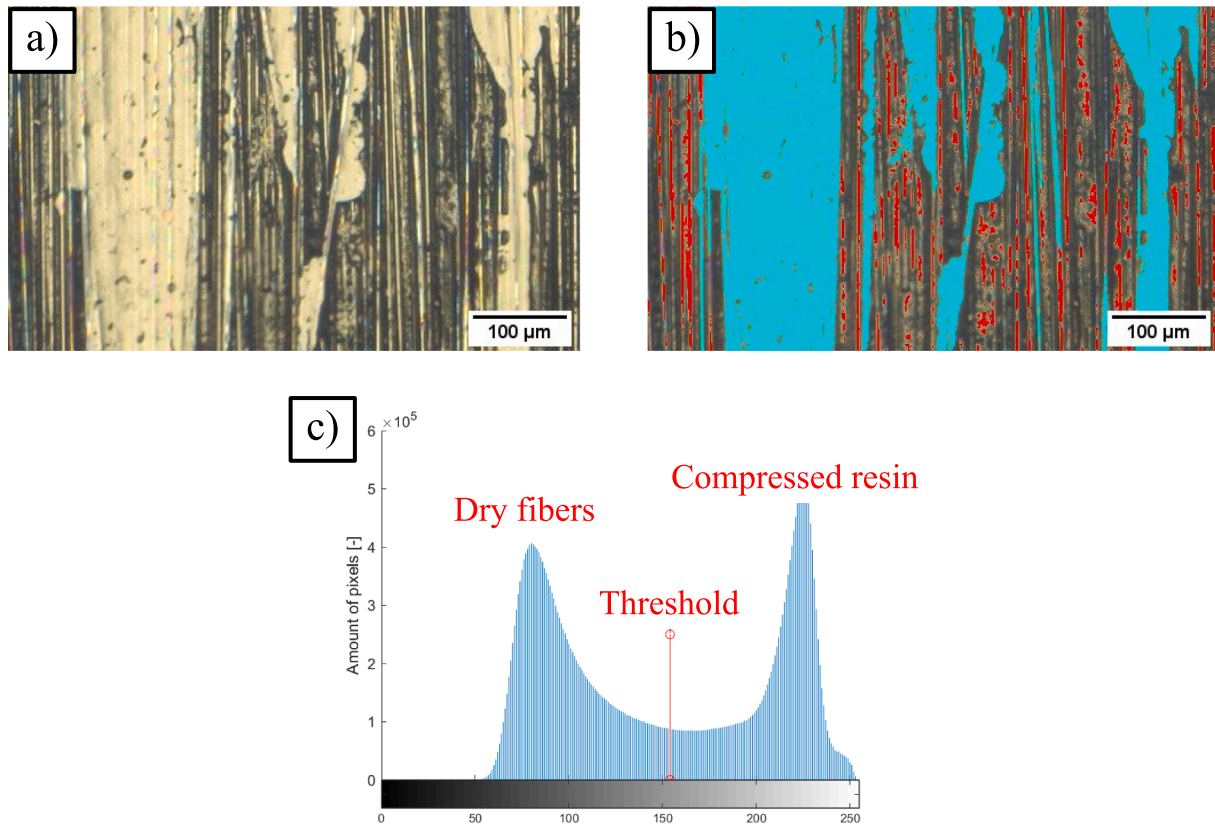


**Fig. 6.** a) A portion of the micrograph of the tape surface after the compaction test, b) Segmented image showing the regions with DEIC (cyan) and regions selected with the histogram but excluded due to minimum size limit (red), c) the grayscale histogram and the minimum threshold to determine the area with DEIC.

equipment. A Keyence VK-X1000 Laser Scanning Confocal Microscope (LSCM) was used to obtain the cross-sectional images. To capture the whole tape width with high resolution, several images were taken and stitched with the  $20\times$  lens in the Focus Variation method. The thickness of each tape was determined using the native software of the instrument. The void content of each tape was manually measured using ImageJ software.

## 2.6. Roughness and waviness

A Keyence VK-X1000 LSCM was used to measure surface roughness and waviness of each specimen before and after the compaction experiments. Three sections (top, middle and bottom) spanning the whole width of the top (laser-irradiated) surface of each specimens were captured. At each section, multiple images were taken in the tape width direction using the  $20\times$  lens and stitched together to form a single confocal image. The size of each section in the fiber direction was the height of a single image, which was approximately 525 μm. 11 primary profiles were extracted from each section.

The primary profiles were filtered to distinguish the roughness and waviness profiles following the ISO 4287 [18] and ISO 4288 [19] standards. The filter required the definition of the cut-off wavelengths  $\lambda_s$ ,  $\lambda_c$  and  $\lambda_f$  shown in Fig. 7. To obtain the roughness profile,  $\lambda_s$  and  $\lambda_c$  were set to 0 mm and 0.8 mm, respectively. To separate the waviness profile from the larger-wavelength components of the surface profile;  $\lambda_f$  was set to 2.5 mm. From this data, root mean square (RMS) roughness ( $R_q$ ) and waviness ( $W_q$ ) were calculated. Additional images of the tapes were taken using a Keyence VR-5000 wide-area 3D measurement system at a low magnification factor of  $12\times$ . These images were used to quickly observe the features on the whole tape surface.

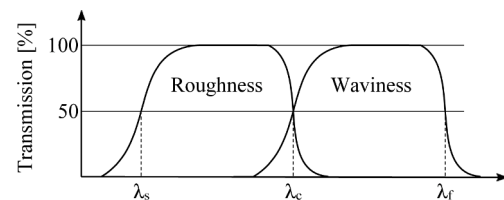


**Fig. 7.** Transmission characteristic of roughness and waviness profiles with the demonstration of cut-off wavelengths  $\lambda_s$ ,  $\lambda_c$  and  $\lambda_f$ . Reproduced from [18].

## 3. Results

### 3.1. Effects of laser-deconsolidation on the structure of the tape before compaction

The laser-deconsolidated tapes had significantly different microstructures compared to the as-received tapes due to deconsolidation mechanisms such as fiber decompaction, void growth, specific volume change and residual stresses [12]. Fig. 8 demonstrates representative cross-sectional micrographs of the ASR, SLD and HLD specimens. As shown in Fig. 8a, the overall shape of the ASR tapes was flat. There was no resin-rich layer at the tape surface; however, the fibers at the surfaces were not detached from the body of the tape. A slight variation in fiber volume fraction was observed throughout the tape but no resin pockets or dry fibers were present. The SLD tapes demonstrated in Fig. 8b, however, contained some forms of deconsolidation such as waviness and a few voids. Such features were rather localized and a major portion of the tape width was unaffected by the laser heating. The most severe signs of deconsolidation were observed in the HLD tapes as pointed out in Fig. 8c. The tape was warped and the thickness of the tape was

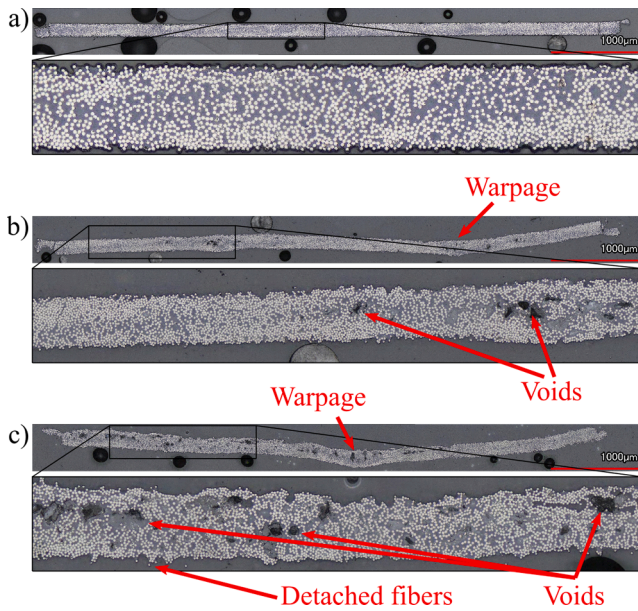


Fig. 8. Representative cross-sectional images of a) as-received, b) slightly laser-deconsolidated, and c) highly laser-deconsolidated samples.

irregular. The void content was much higher than the SLD tapes. Fibers detached from the tape surface were widespread.

Using the cross-sectional micrographs of each sample, the void content of the ASR, SLD and HLD tapes was calculated. Fig. 9a shows the effect of degree of deconsolidation on the void content for samples prepared for experiments at different pressure levels. The ASR tapes had a very low void content ( $< 1\%$ ). However, laser heating resulted in a significant increase in the void content even when the average surface temperature was below  $T_m$  as the SLD tapes had an average void content of 2.8%. The void content of the HLD samples was even higher (4.6% on average), confirming the qualitative observations based on the cross-sectional images.

Laser-deconsolidation also led to an increase in surface roughness as shown in Fig. 10a. As the degree of deconsolidation increased, the surface roughness increased. The difference between the average roughness of the ASR (3.7  $\mu\text{m}$ ) and SLD (5.7  $\mu\text{m}$ ) tapes were around 2  $\mu\text{m}$ . The average roughness of the HLD tapes (10  $\mu\text{m}$ ) was much higher (4.3  $\mu\text{m}$ ) than the SLD tapes.

In addition to the local features at the surface, features of the tape at a larger scale also varied as a result of the warpage and motion of the

fiber bundles after laser heating. This can be seen in the RMS waviness of each degree of deconsolidation presented in Fig. 11a. The ASR tape was practically flat with a very low waviness value, 1  $\mu\text{m}$ . As the degree of deconsolidation increased, the waviness increased significantly. On average, the SLD and HLD tapes had an RMS waviness of 8.2  $\mu\text{m}$  and 13.7  $\mu\text{m}$ , respectively.

The average initial DEIC of the ASR tapes was found to be 5.9%. Unfortunately, it was not possible to measure the initial DEIC of the laser-deconsolidated samples. The surface micrographs were out-of-focus at many locations due to the high amount of out-of-plane deformation. Considering the increased roughness and detached fibers at the surface due to laser-deconsolidation (shown in Fig. 8), it can be expected that the laser-deconsolidated samples have a lower initial DEIC than the ASR samples.

### 3.2. Compaction behavior of the as-received and deconsolidated tapes

#### 3.2.1. In-situ gap thickness

Firstly, the repeatability of the gap thickness measurements of the reference (Kapton-only) experiments was assessed. It was observed that the difference between the gap thickness values from different experiments was below 20  $\mu\text{m}$  under the same pressure. Also, using the averaged reference gap thickness curve for each degree of deconsolidation and temperature/pressure combination reduced the effect of the variation of Kapton-only measurements even further.

In-situ gap thickness of the ASR, SLD and HLD tapes that were heated up to 363  $^{\circ}\text{C}$  were grouped by the applied pressure and presented with the accompanying temperature history in Fig. 12a-d. A common behavior was observed at each pressure level. A significant drop in gap thickness was observed around  $T_g$  for the SLD and HLD tapes at all pressures and the ASR tape at 10 kPa. This sudden decrease was followed by a plateau until  $T_m$ . When  $T_m$  was exceeded, a second large decrease in gap thickness was observed for all samples at each pressure. After this point, the gap thickness decreased slightly further and then stayed practically constant. Based on the overall behavior of the gap thickness curves, three distinct characteristic points were defined and used to compare the samples quantitatively. As demonstrated in Fig. 13, these points are the initial gap, gap after  $T_g$  and the final gap.

Fig. 14a shows the initial gap thickness of the ASR, SLD and HLD tapes. The degree of deconsolidation clearly affected the initial gap thickness at each pressure level. At the pressure of 10 kPa, the initial gap thickness of the ASR, SLD and HLD tapes were around 190, 260 and 320  $\mu\text{m}$ , respectively. It is thought that the low pressure was not sufficient to flatten the overall form of the tape, which was a result of the warpage that occurred during sample extraction. As the pressure was increased to 50 kPa, the warpage was eliminated and the initial gap thickness of the

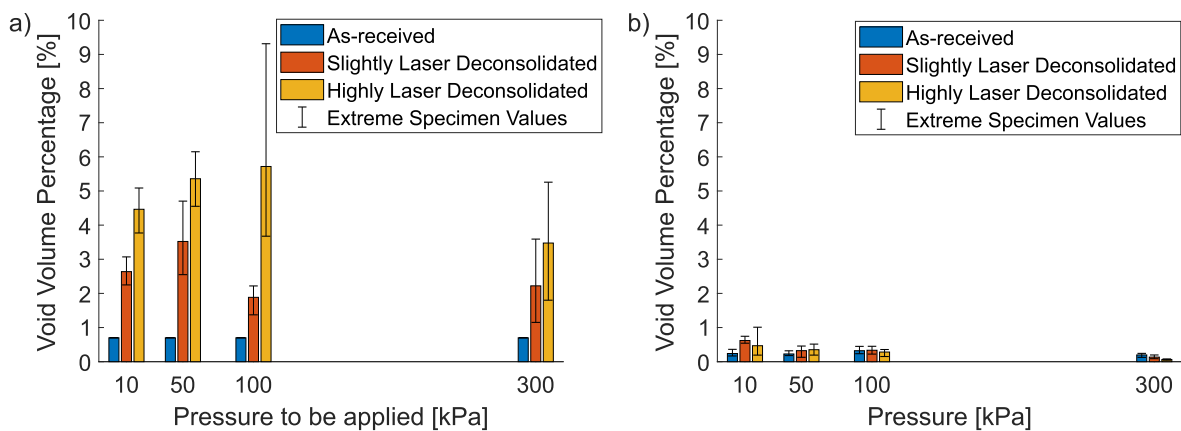
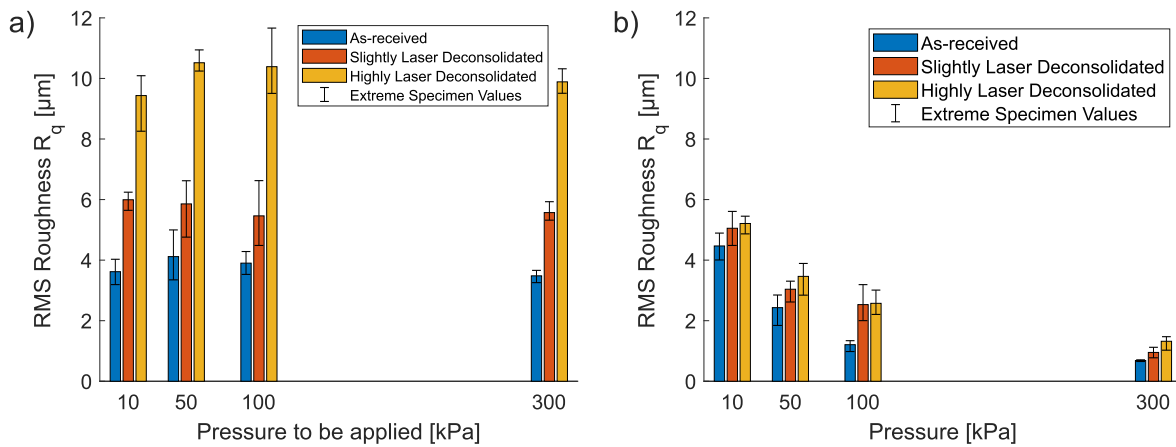
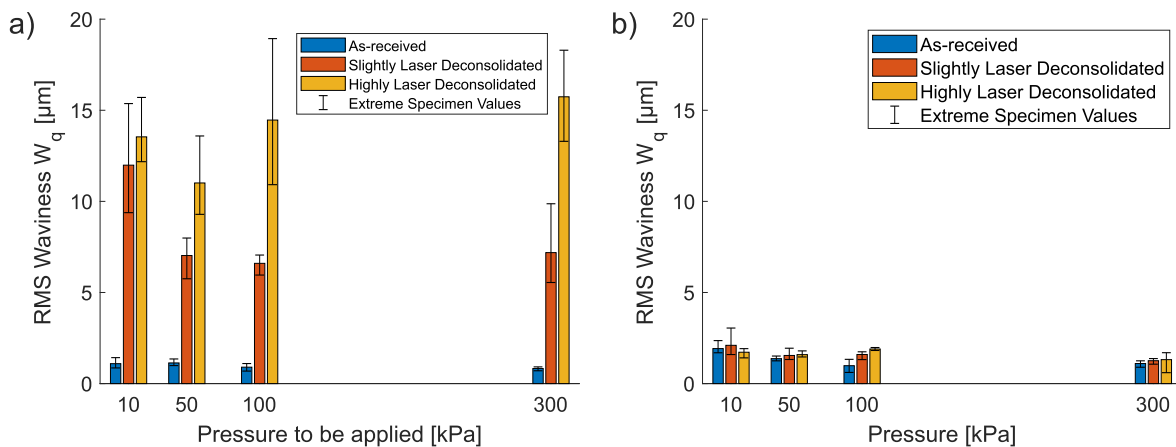


Fig. 9. a) Void content of the as-received (ASR), slightly laser-deconsolidated (SLD), and highly laser-deconsolidated (HLD) samples prior to the experiments with a maximum temperature of 363  $^{\circ}\text{C}$  and pressure levels of 10, 50, 100 and 300 kPa. b) Void content of the samples after being subjected to the respective compaction pressure. The data for ASR tapes in a) is reproduced from [12].



**Fig. 10.** a) RMS roughness of the as-received (ASR), slightly laser-deconsolidated (SLD), and highly laser-deconsolidated (HLD) samples prior to the experiments with a maximum temperature of 363 °C and pressure levels of 10, 50, 100 and 300 kPa. b) RMS roughness of the samples after being subjected to the respective compaction pressure.



**Fig. 11.** a) RMS waviness of the as-received (ASR), slightly laser-deconsolidated (SLD), and highly laser-deconsolidated (HLD) samples prior to the experiments with a maximum temperature of 363 °C and pressure levels of 10, 50, 100 and 300 kPa. b) RMS waviness of the samples after being subjected to the respective compaction pressure.

tapes decreased to  $\sim 150$ , 200 and 300  $\mu\text{m}$  for the ASR, SLD and HLD tapes, respectively. Experiments performed at a pressure of 100 kPa resulted in a slight decrease in the initial gap thickness for ASR and SLD tapes but the difference was small and stayed within the measurement accuracy of the initial gap thicknesses at 50 kPa. At 300 kPa, the initial gap thickness did not change significantly for the ASR and SLD tapes but reduced to  $\sim 240$   $\mu\text{m}$  for the HLD tapes.

Fig. 14b shows the reduced gap thickness after the  $T_g$ . A significant reduction in gap thickness was observed for the HLD samples, ranging between 80 and 150  $\mu\text{m}$  at each pressure level. The gap thickness of the SLD tapes decreased less, within a range of 20–50  $\mu\text{m}$ . The gap thickness of the ASR samples reduced significantly at only 10 kPa and it was around 30  $\mu\text{m}$ . The reduction was below 10  $\mu\text{m}$  for the pressure levels of 50 and 100 kPa and zero at 300 kPa. The SLD and HLD samples had a higher gap thickness than the ASR samples at every pressure level. However, the degree of deconsolidation did not have a significant effect on the gap thickness after  $T_g$  for the laser-deconsolidated samples.

Fig. 14c and d show the final gap thickness and the thickness from the cross-sectional images, respectively, for all samples. It can be seen that the values obtained via the two methods agree with each other very well in general. Only at 10 kPa, the gap length was slightly higher than the thickness, which can be explained by the effect of the overall form of the tape due to the lack of sufficient pressure to keep the tape flat. A comparison of Fig. 14c and Fig. 14b reveals that the SLD and HLD tapes

were compacted significantly from their thickness at  $T_g$  at all pressures, whereas this was the case for the ASR tape at only 300 kPa. Fig. 14d demonstrates that the thickness of all the samples were below the nominal thickness of the ASR tape with the exception of the HLD tape at 10 kPa. The effect of the degree of deconsolidation was minor as the average final thickness of the ASR and HLD tapes differed around 10  $\mu\text{m}$  at most.

The in-situ gap thickness measurements from the experiments with a maximum temperature of 200 °C are shown in Fig. 15. Fig. 15a demonstrates that the gap thickness of the SLD and HLD samples dropped significantly at  $T_g$  as in the previous experiments (shown in Fig. 12). The ASR tape did not go through significant changes as it did not exceed  $T_m$ . Fig. 15b–d show that the gap thickness of the tapes in the experiments with 200 and 363 °C maximum temperature were similar to each other until the  $T_m$  was reached during the 363 °C experiments. Since the samples from the 200 °C experiments cooled down below  $T_g$  shortly after that point (at around 400 s), it can be assumed that their microstructure represents the state of the tape just after  $T_g$ .

### 3.2.2. Morphological analysis

Fig. 16 shows the representative cross-sections of the pristine ASR and HLD specimens and their states after the compaction experiments at a pressure of 300 kPa. Fig. 16b shows that the micro-structure of the ASR tapes changed minimally from the initial state (Fig. 16a) when subjected

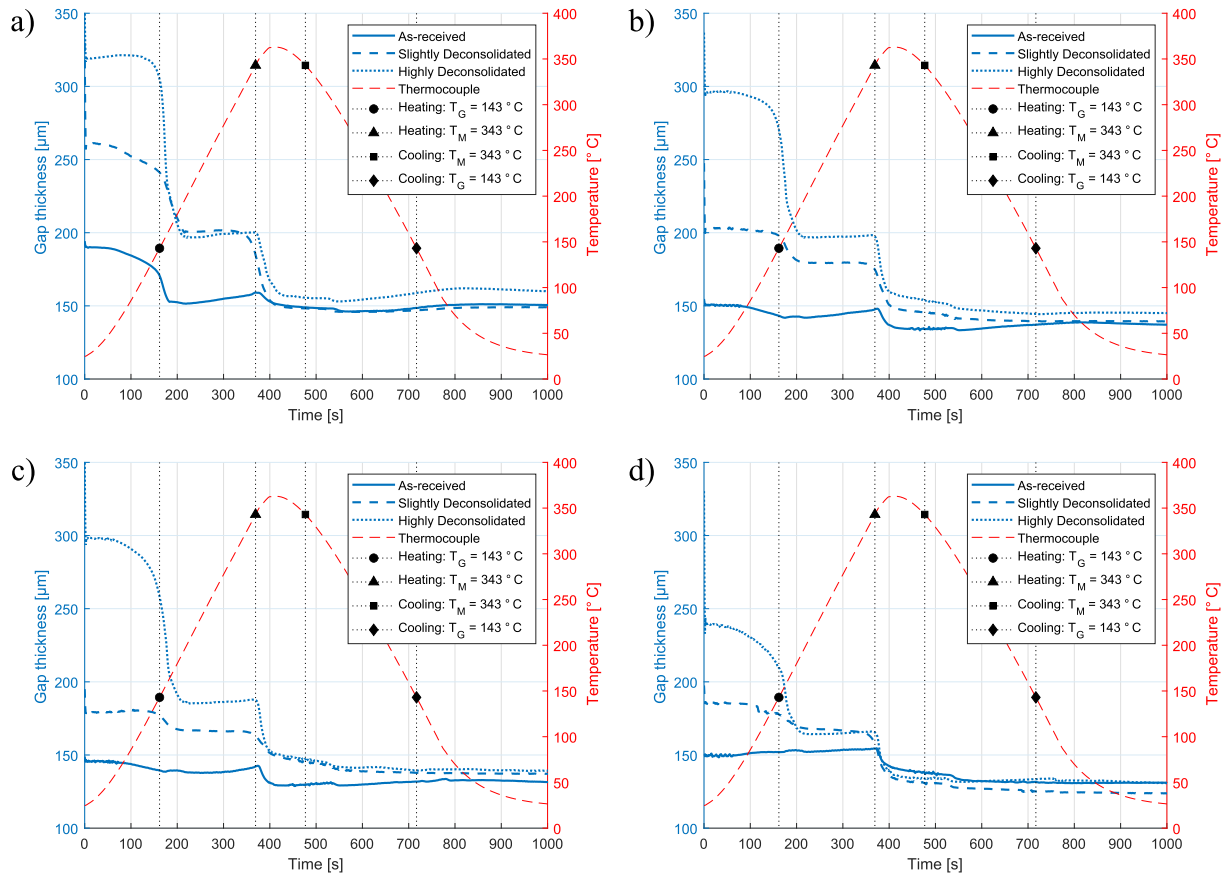


**Fig. 12.** In-situ gap thickness of ASR, SLD and HLD tapes heated up to 363 °C under the pressure of a) 10 kPa, b) 50 kPa, c) 100 kPa and d) 300 kPa. The temperature histories are also added and T<sub>g</sub> and T<sub>m</sub> during heating and cooling are marked.

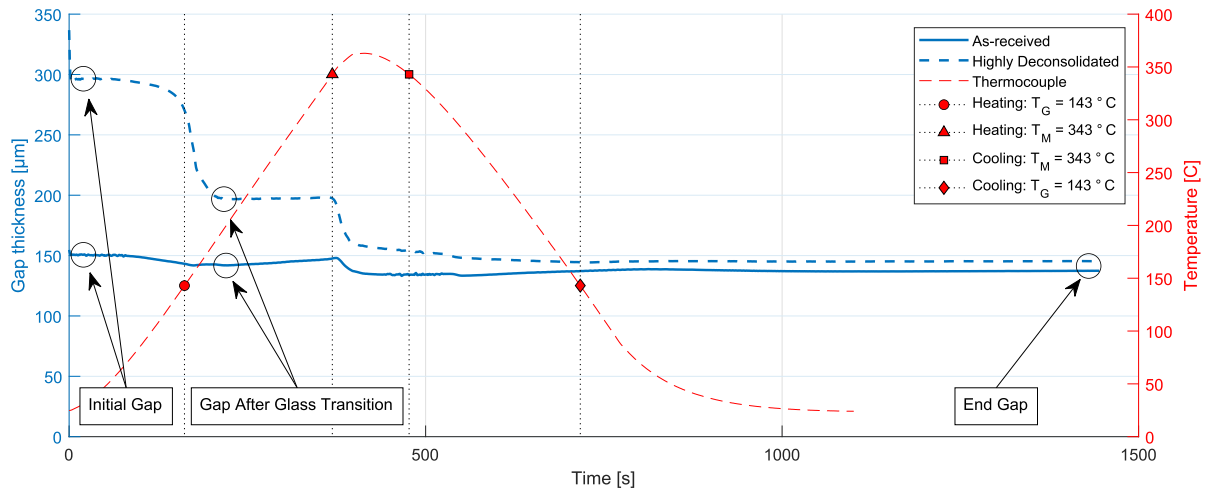


**Fig. 13.** Characteristic points on the gap thickness curves that were selected to compare the samples quantitatively.

to a maximum temperature of 200 °C. The surface features of the tape did not flatten and the thickness did not change much. When compacted above T<sub>m</sub>, the tape surface was much smoother and the thickness decreased, as shown in Fig. 16c.

The effects of the compaction treatments just above T<sub>g</sub> and above T<sub>m</sub> was much more pronounced for the HLD tapes. Samples treated at just above T<sub>g</sub> (Fig. 16e) were much flatter than their initial states (Fig. 16d) in the meso- scale. The waviness and thickness variations were mostly

eliminated. However, the tape surface was still rough and voids were present within the tape. When the samples were compacted above T<sub>m</sub>, the surface was smoothed, voids were compacted and thickness was reduced (Fig. 16e), leading to a state similar to the ASR samples compacted under the same conditions.

Surface micrographs of the tapes compacted above T<sub>m</sub> provided further information about the polymer flow at the tape surface during compaction. Fig. 17 demonstrates that molten resin flowed significantly

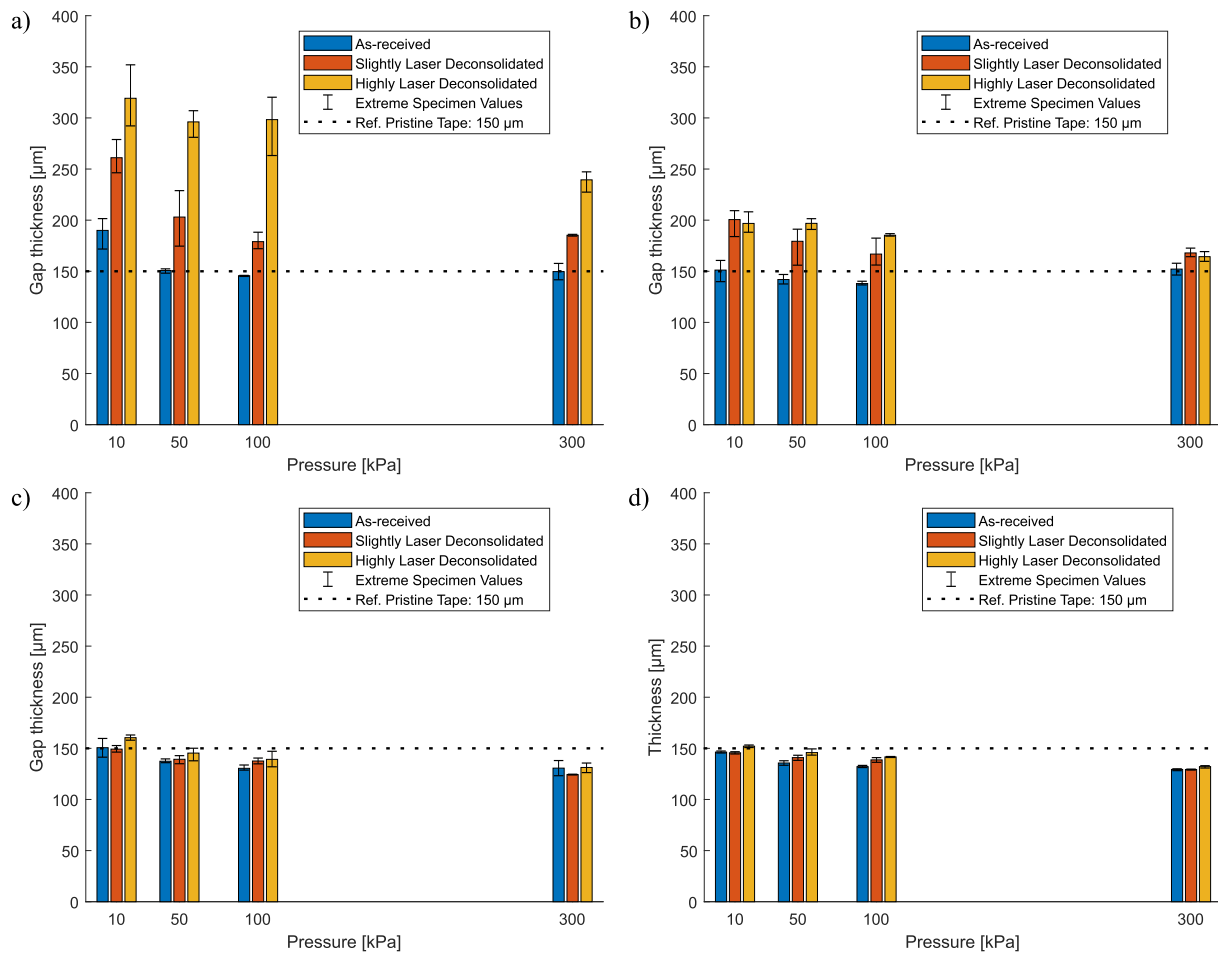


**Fig. 14.** a) The initial gap thickness, b) gap thickness after  $T_g$ , c) final gap thickness and d) thickness from cross-sectional microscopy for the ASR, SLD and HLD tapes subjected to different pressures with a maximum temperature of 363 °C.

in the fiber direction and squeezed out from the edges of the tape. This mode of polymer flow was observed for all samples and the amount of squeezed-out resin increased with increasing pressure.

### 3.2.3. Void content

The final void content of the samples which were compacted above  $T_m$  is shown in Fig. 9b. At 10 kPa, the SLD samples had a slightly higher average void content than the ASR samples. However, a relatively high scatter was observed for the HLD samples, ranging between 0.1 and 1%. At higher pressures, all samples had a similar average final void content between 0.1 and 0.4%. It should be noted that even at 10 kPa, the final void content was below 1%, which is considered a low and tolerable value in industry applications [20].

Fig. 18 shows the final void content of the samples subjected to a maximum temperature of 200 and 363 °C under a pressure of 300 kPa. Compaction just above the  $T_g$  led to reduction of voids, as the void content of ASR, SLD and HLD samples decreased for 0.4, 0.7 and 1.6% on average. However, the voids were not completely eliminated. The degree of deconsolidation had an effect on the void content just above  $T_g$  and the SLD and HLD tapes had a significantly higher void content than the ASR tapes. However, when the  $T_m$  was exceeded, the compaction cycle was sufficient to eliminate the voids and all three degrees of deconsolidation resulted in the same, very low amount of void content.

### 3.2.4. Effective intimate contact

The final degree of effective intimate contact (DEIC) of the ASR, SLD and HLD tapes subjected to 363 °C is shown in Fig. 19. The effect of both the pressure and the degree of deconsolidation can be observed in the

results. An increase in the applied pressure increased the DEIC for all degrees of deconsolidation. Even at the lowest pressure setting (10 kPa), the DEIC was significant (45–50% for the ASR tape and 35–45% for the SLD and HLD tapes) for all samples. At the highest pressure (300 kPa), all samples reached an average DEIC of ~85%. The effect of the degree of deconsolidation was apparent at pressures below 300 kPa. The average DEIC decreased as the degree of deconsolidation increased.

Fig. 20 shows the final DEIC of the samples subjected to a maximum temperature of 200 and 363 °C under a pressure of 300 kPa. Unlike the samples that were compacted above  $T_m$ , the samples compacted just above  $T_g$  had a very low final DEIC. Also, the degree of deconsolidation did not affect the DEIC just after  $T_g$ .

### 3.2.5. Surface roughness

The final RMS roughness of the samples subjected to a maximum temperature of 363 °C is shown in Fig. 10b. The degree of deconsolidation had an effect at every pressure level. The mean roughness of the SLD and HLD tapes was higher than the ASR tapes. The HLD samples were slightly rougher than the SLD samples on average; however, due to scatter, no clear distinction can be made. The effect of pressure was also apparent for all degrees of deconsolidation. As the pressure increased, the roughness decreased. At 10 kPa, the roughness of the ASR tape was slightly higher than its initial value shown in Fig. 10a; however, the roughness of the laser-deconsolidated tapes, especially the HLD ones, decreased significantly.

Fig. 21 shows the final RMS roughness of the samples subjected to a maximum temperature of 200 and 363 °C under a pressure of 300 kPa. During the 200 °C experiments, the surface features of the tapes were not

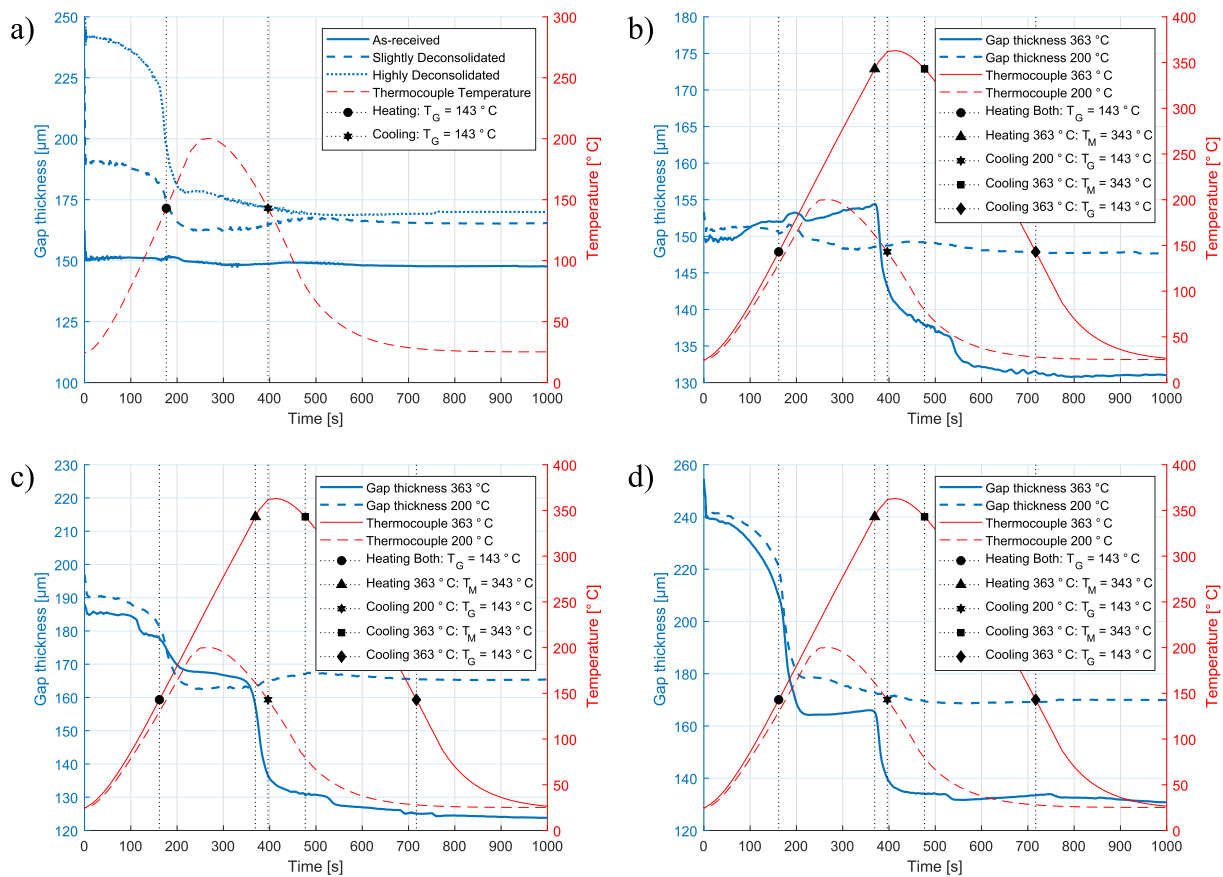


Fig. 15. In-situ gap thickness of a) ASR, SLD and HLD tapes heated up to 200 °C under the pressure of 300 kPa and comparison between b) ASR tapes, c) SLD tapes and d) HLD tapes heated up to 200 °C and 363 °C under the pressure of 300 kPa.

flattened as much as the 363 °C experiments, which is shown by the higher roughness values. For the samples subjected to 200 °C, the roughness increased as the degree of deconsolidation increased. It should be noted that the roughness of the ASR tapes did not change significantly from the initial value, whereas a reduction of 1.1  $\mu\text{m}$  and 4.1  $\mu\text{m}$  was observed for the SLD and HLD tapes, respectively. All of the samples which were subjected to 363 °C reached a roughness which is smaller than the initial roughness of the ASR tape. The difference between the degrees of deconsolidation was much less compared to the samples subjected to a maximum temperature of 200 °C.

### 3.2.6. Waviness

The final RMS waviness of the samples subjected to a maximum temperature of 363 °C is shown in Fig. 11b. It can be seen that all of the samples had a significantly reduced waviness at the end of the experiments compared to their initial waviness (shown in Fig. 11a). The degree of deconsolidation and pressure seem not to have a significant effect on the final waviness. Only at 10 kPa, the waviness of the ASR tape was slightly higher than its initial value.

Fig. 22 compares the final RMS waviness of the samples subjected to a maximum temperature of 200 and 363 °C under the pressure of 300 kPa. Confirming the micrographs in Fig. 16, the low RMS waviness values for the samples subjected to 200 °C show the flattening of *meso*-scale features of the tape surface at  $T_g$ . Past the  $T_g$ , the SLD and HLD samples had slightly more waviness than the ASR tapes; however, the difference was minute. The waviness reduced a bit further for all samples subjected to 363 °C and the degree of deconsolidation did not affect the results.

## 4. Discussion

### 4.1. Influence of laser-deconsolidation on the compaction behavior

As explained in Section 3.1, laser-deconsolidation increases the void content, roughness and waviness of the tape. This study shows that such micro-structural changes affect the compaction process of the thermoplastic composite tapes in a number of ways. The effects can be grouped under three temperature ranges: between the room temperature and  $T_g$ , between  $T_g$  and  $T_m$  and above  $T_m$ . The severity of the effects varies in each temperature range.

At room temperature, the waviness of the samples and the thickness increase induced by void growth and fiber decompaction due to laser-deconsolidation were the main reasons of the difference in the gap thickness shown in Figs. 12 and 15. The sudden decrease in the gap thickness when the  $T_g$  was exceeded suggests that the tapes were significantly deformed even if the resin was not in the molten state. The cross-sectional micrographs of the HLD samples shown in Fig. 16e and the final waviness values of the samples subjected to a maximum temperature of 200 °C reported in Fig. 22 suggest that the waviness was eliminated at the  $T_g$ . Unlike waviness, the voids and surface roughness were reduced but not completely eliminated (shown in Figs. 18 and 21, respectively). At the  $T_g$ , the storage modulus of CF/PEEK decreases significantly and PEEK transforms into the rubbery state [21]. This transition is sufficient to flatten the *meso*-scale features of the tape even under very low pressures but fails to fill in the voids or cause them to migrate out of the tape completely, or establish effective intimate contact at the surface.

Between the  $T_g$  and  $T_m$ , the in-situ gap thickness measurements in

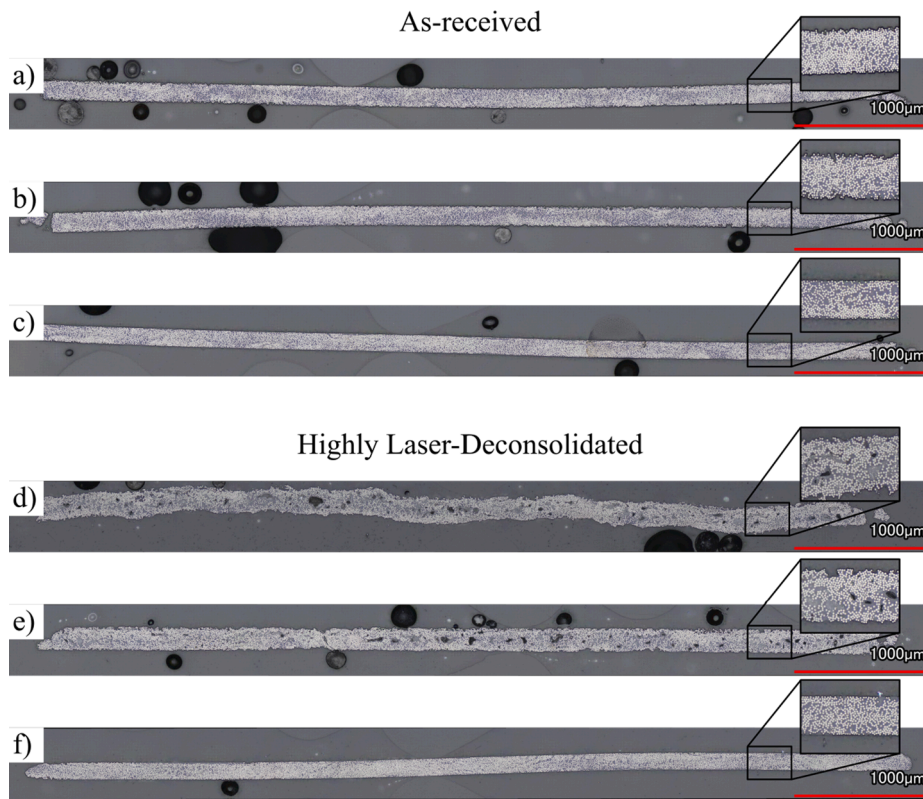


**Fig. 16.** Representative cross-sectional images of the ASR and HLD tapes before the compaction experiments (a and d)), after being subjected to a maximum temperature of 200 °C and 300 kPa (b and e)) and after being subjected to a maximum temperature of 363 °C and 300 kPa. a)–b) and d)–e) are from different locations of the same specimen.

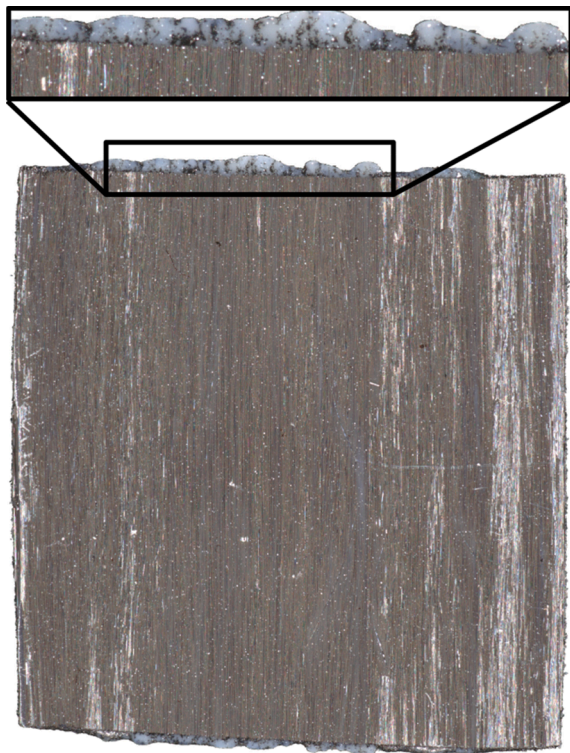


**Fig. 17.** Surface micrograph of an HLD tape subjected to a maximum temperature of 363 °C and a pressure of 300 kPa demonstrating the squeezed-out resin in the fiber direction.

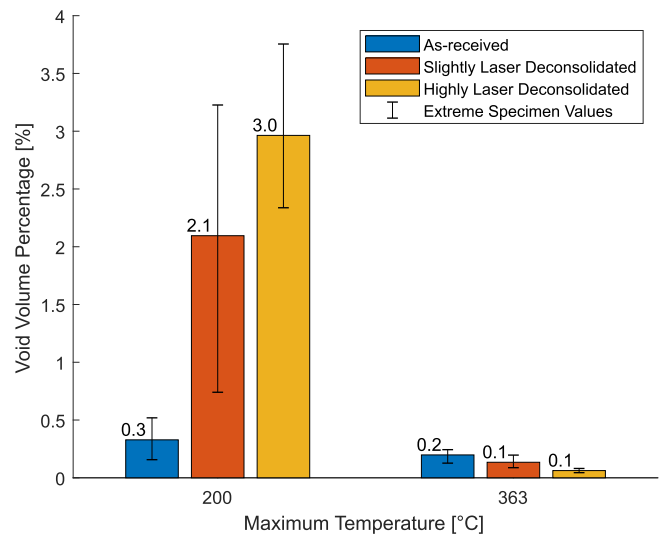


**Fig. 18.** Final void content of the ASR, SLD and HLD specimens subjected to a maximum temperature of 200 and 363 °C and pressure of 300 kPa. Initial average void content of ASR: 0.7 %, SLD: 2.8 %, HLD: 4.6 %.

Fig. 12 show no sign of change in the micro-structure of the as-received and deconsolidated tapes regardless of the applied compaction pressure. It is thought that the void content and surface roughness of the tapes just above the  $T_g$  stay almost constant in this phase since the change of the gap thickness is on the order of few microns. Thus, it can be stated that the microscopic effects of laser-deconsolidation cannot be completely eliminated if the resin is not in a molten state.

When the  $T_m$  was exceeded during compaction, the difference

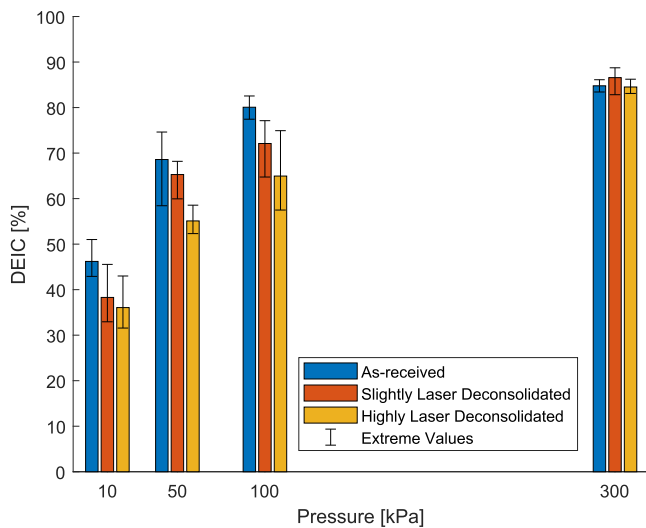


Fig. 19. The final degree of effective intimate contact for the ASR, SLD and HLD samples subjected to a maximum temperature of 363 °C.

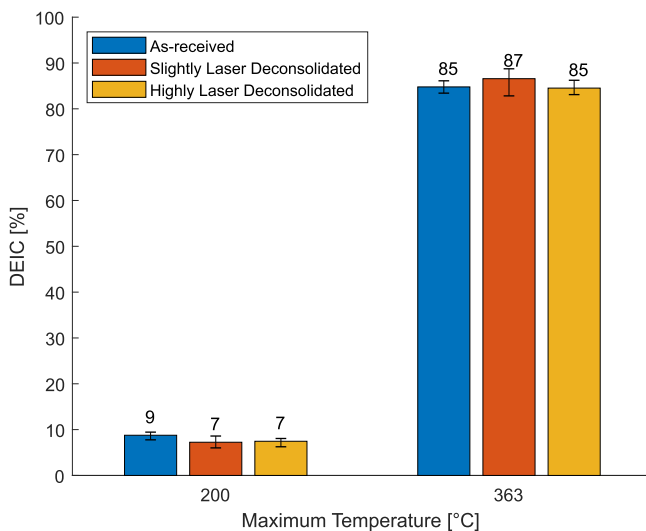


Fig. 20. The final degree of effective intimate contact for the ASR, SLD and HLD samples subjected to a pressure of 300 kPa and a maximum temperature of 200 °C and 363 °C. The initial average DEIC of ASR: 5.9 %, SLD and HLD are not available but expected to be lower than the DEIC of ASR.

between the in-situ gap thickness curves of the as-received and laser-deconsolidated tapes decreased first rapidly, then gradually as shown in Fig. 12. It is thought that the decrease in the difference is dominated by void compaction, as the trend in gap thickness shows resemblance with the calculated decrease of the void content in a tape with a void content of 2 % and a void spacing smaller than 4 mm [6]. Another supporting aspect is that the size of the large voids are larger than the surface asperities after the  $T_g$  as shown in Fig. 16e. As depicted in Fig. 9b and Fig. 16f, the majority of these voids were compacted. Along with void compaction, effective intimate contact was also established due to flow of the molten polymer to the tape surface, as demonstrated in Fig. 19.

Furthermore, qualitative observations on the tape surface (Fig. 17) demonstrated significant polymer flow in the fiber direction. This is thought to be a result of the higher permeability in the fiber direction compared to the direction perpendicular to the fibers and supports the previous findings of the authors [5]. This phenomenon has been neglected in the squeeze-flow based intimate contact models such as Lee

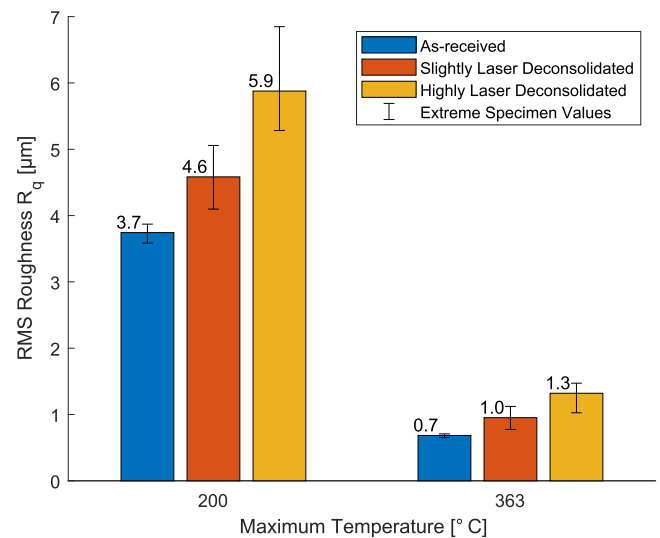


Fig. 21. The final RMS roughness of the ASR, SLD and HLD samples subjected to a pressure of 300 kPa and a maximum temperature of 200 °C and 363 °C. Initial average RMS roughness of ASR: 3.7 µm, SLD: 5.7 µm, HLD: 10.0 µm.

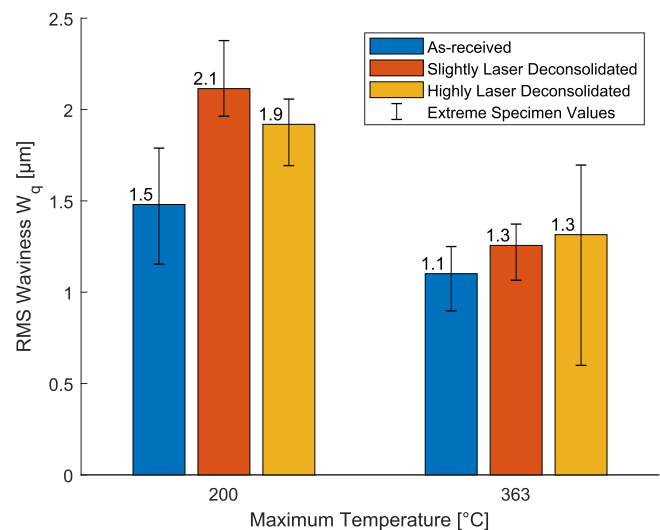


Fig. 22. The final RMS waviness of the ASR, SLD and HLD samples subjected to a pressure of 300 kPa and a maximum temperature of 200 °C and 363 °C. Initial average RMS waviness of ASR: 1 µm, SLD: 8.2 µm, HLD: 13.7 µm.

and Springer [3] and Yang and Pitchumani [4], as they have only considered polymer flow in the direction perpendicular to the fibers. For a more accurate description of effective intimate contact development, resin flow in the fiber direction should be considered.

#### 4.2. Significance for the LAFP process

Among the abovementioned effects of laser-deconsolidation, the gap thickness after  $T_g$  (Fig. 14b), RMS roughness (Fig. 10b) and DEIC (Fig. 19) showed dependence to the level of applied pressure. Below a pressure of 300 kPa, the influence of laser-deconsolidation was apparent in terms of an increased thickness after  $T_g$ , increased RMS roughness, and decreased DEIC. In [5], it is reported that a compaction pressure above 300 kPa can be reached even with low levels of compaction force on flat surfaces. However, the pressure under the compaction roller is determined by the mechanical properties of the roller and softer rubbers might require higher compaction forces to reach that pressure level. Also, moulds with non-flat surfaces have been increasingly used, as

LAFP can be used to manufacture structures such as fuselage panels [22], variable-stiffness wingboxes [23] or pressure vessels [24]. During the material deposition on these surfaces, a reduction of the compaction pressure might occur between the contact points of concave surfaces [25] or the roller not conforming with the complete tow at corners [23]. It is suggested that laser-deconsolidation should be especially considered for such applications, as the regions with decreased pressure are susceptible to its effects.

Recent works showed that intimate contact can develop significantly between  $T_g$  and  $T_m$  for CF/PEEK laminates manufactured with LAFP [26] and CF/PEKK laminates manufactured with out-of-autoclave consolidation [27]. This was not the case during the compaction experiments performed at a maximum temperature of 200 °C, as shown in Fig. 20. Two reasons can be identified for the difference between the experimental results and the literature. The first one is the temperature level reached during compaction. In [26], the nip point temperature was between 310–330 °C, whereas in [27], the CF/PEKK composite, whose  $T_m$  was 335 °C, was heated to 230 °C. In both studies, the maximum temperature was closer to the  $T_m$  of the material than it was in this study, which might have allowed more deformation of the surface asperities. The second reason concerns the scale of the surface deformation required for the development of intimate contact. So far, the existing squeeze flow-based intimate contact models [3,4] considered the intimate contact phenomenon to occur at the scale of the roughness profile of the surface. However, Fig. 16e shows that it is the waviness profile of the tape which deforms significantly past the  $T_g$ . Such a result suggests that flattening of the waviness of the tape plays a role in intimate contact development and can be a key element for a more accurate intimate contact model for LAFP.

The compaction behavior of the laser-deconsolidated tapes during the experiments leads to additional novel insights for the compaction phase of the actual LAFP process. Firstly, the significant reduction of laser-induced waviness above the  $T_g$  means that pressure variation along the width of the tape due to local contact of the tape–substrate and tape–compaction roller at the peaks and valleys of the waviness profile can be neglected since the temperature of the tape usually exceeds the  $T_g$ . Nevertheless, the laser-induced voids and surface roughness are expected to be present above the  $T_g$  and might play a role in the final quality of the part. Given that the tape might be compacted between the  $T_g$  and  $T_m$  during LAFP due to rapid heat dissipation [16], several phenomena would be affected by this micro-structural difference. Firstly, the amount of voids that need to be compacted can be an order of magnitude higher than the ASR tape, as suggested by Fig. 18. This is crucial for the calculation of the final void content since the void content at the beginning of compaction is an important parameter for void filling models [6,7]. Additionally, heat transfer mechanisms during the compaction phase are expected to be influenced by the difference between the as-received and laser-deconsolidated states. As shown in Fig. 14b, the laser-deconsolidated samples were thicker than the as-received tapes significantly: ~30 % at pressures below 300 kPa and ~15 % at 300 kPa. Also, the voids and the rough tape surface would increase the intra- and inter-layer thermal resistance. These effects would influence the temperature gradient within the tape and the heat flux between the tape and surrounding bodies (the compaction roller and substrate) and should be considered for a more accurate analysis of the temperature history during the compaction phase of LAFP. Finally, if sufficient dwell time is allowed above  $T_m$ , the voids and surface roughness due to laser-deconsolidation can be remedied. During LAFP, raising the tape temperature high enough so that it stays above the  $T_m$  at the beginning of compaction (past the shadow prior to the nip point) can be a viable option to reduce the effects of laser-deconsolidation. However, it should be ensured that the temperature of the newly placed tape is lower than the  $T_g$  at the roller exit (i.e. by means of active cooling systems such as convective air cooling, a secondary cooling roller or water cooling for the compaction roller [29]) so that further deconsolidation is prevented during the cooling phase.

#### 4.3. Limitations of the current work

The results presented in this work provide important insight that can be reflected to the actual LAFP process; however, it should be noted that the laser-deconsolidation and compaction experiments presented in this work may deviate from the heating and compaction phases of the LAFP process. Firstly, during the laser-deconsolidation experiments explained in Section 2.2, the CF/PEEK tapes were heated in a static setting. In an actual LAFP process, the incoming tape moves across a fixed laser-illuminated zone with the programmed placement speed as shown in Fig. 1. This might change the through-thickness temperature gradient and hence, the extent of the effects of deconsolidation in the thickness direction. In the static setup, the heat can diffuse much more towards the non-irradiated surface of the tape and lead to more deconsolidation. Considering the difference in through-thickness temperature gradient, it can be stated that the HLD specimens represent a worst-case scenario for the state of the tape at the nip point in an actual LAFP process. Moreover, one should be aware of the fact that the time spent at temperatures near the  $T_m$  of the material during the compaction experiments (although it was shorter than conventional composite processing times, which is on the order of several minutes) was significantly longer than the actual compaction phase of the LAFP process. As a result, the effects of the degree of deconsolidation on surface roughness, DEIC and void content can be even more pronounced during the actual LAFP process. In terms of the compaction time, the results from the samples which were subjected to a maximum temperature of 363 °C represent the best-case scenario for LAFP.

#### 5. Conclusion

This study investigates the effects of laser-deconsolidation on the compaction process of CF/PEEK tapes experimentally. A two-step experimental procedure was performed. In the first step, a VCSEL heater was utilized to deconsolidate composite tapes under conditions similar to the heating phase of LAFP. Samples with two degrees of deconsolidation, which differed by the surface roughness, waviness and void content from the as-received tapes, were obtained using two different laser power settings. In the second step of experiments, the as-received and laser-deconsolidated tapes were compacted under different temperature and pressure settings. In-situ measurement of the gap thickness during compaction and ex-situ measurement of surface profile, degree of effective intimate contact and void content were used to assess the effects of laser-deconsolidation.

The results have shown that waviness induced by laser-deconsolidation vanishes when the material is heated up to the glass transition temperature even at a very low compaction pressure. This suggests that the compaction phase of LAFP would not be affected by the meso-scale deformations in the tape due to laser heating since the material is usually heated above its glass transition temperature. Unlike waviness; increased thickness, void content and surface roughness due to laser-deconsolidation remained between the glass transition and melting temperatures. These forms of deconsolidation were removed only above the melting temperature. This shows the importance of increasing the temperature of the material before the nip point high enough so that it stays above the melting temperature for a duration under the compaction roller, provided that it is cooled down below the glass transition temperature at the roller exit. Applied pressure also plays a significant role in the final properties of the compacted tapes. The final surface roughness and degree of effective intimate contact were affected by the laser-deconsolidation when a compaction pressure less than 300 kPa was applied. For future work, it is suggested that the effects of laser-deconsolidation are considered in process models, especially for process settings which do not ensure that the tape stays above the melting temperature under the compaction roller.

## CRedit authorship contribution statement

**Ozan Çelik:** Conceptualization, Methodology, Formal analysis, Visualization, Data curation, Writing – original draft, Writing – review & editing. **Tom Bussink:** Conceptualization, Methodology, Investigation, Formal analysis, Visualization, Data curation. **Daniël Peeters:** Writing – review & editing, Resources, Supervision. **Julie Teuwen:** Conceptualization, Methodology, Writing – review & editing, Resources, Supervision. **Clemens Dransfeld:** Writing – review & editing, Resources, Supervision.

## Declaration of Competing Interest

The authors declare that they have no known competing financial interests or personal relationships that could have appeared to influence the work reported in this paper.

## References

- [1] Chanteli A, Bandaru AK, Peeters D, O'Higgins RM, Weaver PM. Influence of repass treatment on carbon fibre-reinforced PEEK composites manufactured using laser-assisted automatic tape placement. *Compos Struct* 2020;248:112539. <https://doi.org/10.1016/j.compstruct.2020.112539>.
- [2] Kozaczuk K. Automated Fiber Placement Systems Overview. *Trans Instit Aviation* 2016;245(4):52–9. <https://doi.org/10.5604/05096669.1226355>.
- [3] Lee WI, Springer GS. A Model of the Manufacturing Process of Thermoplastic Matrix Composites. *J Compos Mater* 1987;21(11):1017–55. <https://doi.org/10.1177/002199838702101103>.
- [4] Yang F, Pitchumani R. A fractal Cantor set based description of interlaminar contact evolution during thermoplastic composites processing. *J Mater Sci* 2001;36(19):4661–71. <https://doi.org/10.1023/A:1017950215945>.
- [5] Çelik O, Peeters D, Dransfeld C, Teuwen J. Intimate contact development during laser assisted fiber placement: Microstructure and effect of process parameters. *Compos A Appl Sci Manuf* 2020;134:105888. <https://doi.org/10.1016/j.compositesa.2020.105888>.
- [6] Simacek P, Advani SG, Gruber MB, Jensen B. A non-local void filling model to describe its dynamics during processing thermoplastic composites. *Compos A Appl Sci Manuf* 2013;46(1):154–65. <https://doi.org/10.1016/j.compositesa.2012.10.015>.
- [7] Pitchumani R, Ranganathan S, Don RC, Gillespie JW, Lamontia MA. Analysis of Transport Phenomena Governing Interfacial Bonding and Void Dynamics During Thermoplastic Tow-placement. *Int J Heat Mass Transf* 1996;39(9):1883–97. [https://doi.org/10.1016/0017-9310\(95\)00271-5](https://doi.org/10.1016/0017-9310(95)00271-5).
- [8] Khan MA, Mitschang P, Schledjewski R. Parametric study on processing parameters and resulting part quality through thermoplastic tape placement process. *J Compos Mater* 2013;47(4):485–99. <https://doi.org/10.1177/0021998312441810>.
- [9] Comer AJ, Ray D, Obando WO, Jones D, Lyons J, Rosca I, et al. Mechanical characterisation of carbon fibre-PEEK manufactured by laser-assisted automated-tape-placement and autoclave. *Compos A Appl Sci Manuf* 2015;69:10–20. <https://doi.org/10.1016/j.compositesa.2014.10.003>.
- [10] Jiang J, He Y, Wang H, Ke Y. Modeling and experimental validation of compaction pressure distribution for automated fiber placement. *Compos Struct* 2021;256:113101. <https://doi.org/10.1016/j.compstruct.2020.113101>.
- [11] Henninger F, Ye L, Friedrich K. Deconsolidation behaviour of glass fibre-polyamide 12 composite sheet material during post-processing. *Plast Rubber Compos Process Appl* 1998;27(6):287–92.
- [12] Çelik O, Choudhary A, Peeters D, Teuwen J, Dransfeld C. Deconsolidation of thermoplastic prepreg tapes during rapid laser heating. *Compos A Appl Sci Manuf* 2021;149:106575. <https://doi.org/10.1016/j.compositesa.2021.106575>.
- [13] Kok T, Groupe WJB, Warnet LL, Akkerman R. Intimate Contact Development in Laser Assisted Fiber Placement. In: *ECCM17 - 17th European Conference on Composite Materials* 2016;1(June):26–30.
- [14] Kok T. On the consolidation quality in laser assisted fiber placement: the role of the heating phase. Phd thesis; University of Twente; 2018. doi:10.3990/1.9789036546065.
- [15] Composites TA. TenCate Cetex® TC1200 PEEK Resin System Product Data Sheet 2017.
- [16] Stokes-Griffin CM, Compston P. Investigation of sub-melt temperature bonding of carbon-fibre/PEEK in an automated laser tape placement process. *Compos A Appl Sci Manuf* 2016;84:17–25. <https://doi.org/10.1016/j.compositesa.2015.12.019>.
- [17] Jiang J, He Y, Ke Y. Pressure distribution for automated fiber placement and design optimization of compaction rollers. *J Reinf Plast Compos* 2019;38(18):860–70. <https://doi.org/10.1177/0731684419850896>.
- [18] ISO 4287:1997. Geometrical Product Specifications (GPS) – Surface texture: Profile method – Terms, definitions and surface texture parameters. International Organization for Standardization 1997.
- [19] International Organization for Standardization. ISO 4288:1996 Geometrical Product Specifications (GPS) - Surface texture: Profile method - Rules and procedures for the assessment of surface texture. 1996.
- [20] Mehdikhani M, Gorbatikh L, Verpoest I, Lomov SV. Voids in fiber-reinforced polymer composites: A review on their formation, characteristics, and effects on mechanical performance. *J Compos Mater* 2019;53(12):1579–669. <https://doi.org/10.1177/0021998318772152>.
- [21] Zheng B, Gao X, Li M, Deng T, Huang Z, Zhou H, et al. Formability and failure mechanisms of woven CF/PEEK composite sheet in solid-state thermoforming. *Polymers* 2019;11(6):966. <https://doi.org/10.3390/polym11060966>.
- [22] Rodriguez-Lence F, Martin MI, Fernandez Horcajo K. In-situ consolidation of integrated thermoplastic fuselage panels: The future in structural commercial aerocomposites. In: *ECCM 2018 - 18th European Conference on Composite Materials*. ISBN 9781510896932; 2018.
- [23] Peeters D, Clancy G, Oliveri V, O'Higgins R, Jones D, Weaver PM. Concurrent design and manufacture of a thermoplastic composite stiffener. *Compos Struct* 2019;212:271–80.
- [24] Hosseini SMA, Schäkel M, Baran I, Janssen H, van Drongelen M, Akkerman R. A new global kinematic-optical-thermal process model for laser-assisted tape winding with an application to helical-wound pressure vessel. *Mater Des* 2020;193:108854. <https://doi.org/10.1016/j.matdes.2020.108854>.
- [25] Lichtinger R, Lacalle J, Hinterhölzl R, Beier U, Drechsler K. Simulation and experimental validation of gaps and bridging in the automated fiber placement process. *Sci. Eng. Composite Mater.* 2015;22(2):131–48.
- [26] Çelik O, Hosseini SMA, Baran I, Groupe WJB, Akkerman R, Peeters DMJ, et al. The Influence of Inter-laminar Thermal Contact Resistance on the Cooling of Material during Laser Assisted Fiber Placement. *Compos A Appl Sci Manuf* 2021;145:106367. <https://doi.org/10.1016/j.compositesa.2021.106367>.
- [27] Saffar F, Sonnenfeld C, Beauchêne P, Park CH. In-situ Monitoring of the Out-Of-Autoclave Consolidation of Carbon / Poly-Ether-Ketone- Ketone Prepreg Laminate. *Front Mater* 2020;7(June):1–12. <https://doi.org/10.3389/fmats.2020.00195>.
- [28] Henne F, Ehard S, Kollmannsberger A, Hoeck B, Sause MGR, Drechsler K. Thermoplastic in situ fiber placement for future solid rocket motor casing manufacturing. In: *SAMPE Europe SETEC 14 - Efficient composite solutions to foster economic growth*; 2014;(September 2014)..